Dynamical traps lead to the slowing down of intramolecular vibrational energy flow

Paranjothy Manikandan[1] and Srihari Keshavamurthy[2]

Department of Chemistry, Indian Institute of Technology, Kanpur (U.P.) 208016, India

Edited* by Peter G. Wolynes, Rice University, Houston, TX, and approved August 22, 2014 (received for review April 11, 2014)

The phenomenon of intramolecular vibrational energy redistribution (IVR) is at the heart of chemical reaction dynamics. Statistical rate theories, assuming instantaneous IVR, predict exponential decay of the population with the properties of the transition state essentially determining the mechanism. However, there is growing evidence that IVR competes with the reaction timescales, resulting in deviations from the exponential rate law. Dynamics cannot be ignored in such cases for understanding the reaction mechanisms. Significant insights in this context have come from the state space model of IVR, which predicts power law behavior for the rates with the power law exponent, an effective state space dimensionality, being a measure of the nature and extent of the IVR dynamics. However, whether the effective IVR dimensionality can vary with time and whether the mechanism for the variation is of purely quantum or classical origins are issues that remain unresolved. Such multiple power law scalings can lead to surprising mode specificity in the system, even above the threshold for facile IVR. In this work, choosing the well-studied thiophosgene molecule as an example, we establish the anisotropic and anomalous nature of the quantum IVR dynamics and show that multiple power law scalings do manifest in the system. More importantly, we show that the mechanism of the observed multiple power law scaling has classical origins due to a combination of trapping near resonance junctions in the network of classical nonlinear resonances at short to intermediate times and the influence of weak higher-order resonances at relatively longer times.

phase space | wavelets | Arnold web | Fermi resonance | mode specificity

Understanding, quantifying, and manipulating chemical reactions have been holy grails of chemical physics for nearly a century. In this continuing quest a fundamental and formidable phenomenon that needs to be reckoned with is that of intramolecular vibrational energy redistribution (IVR) (1–5). Although models of reaction rates like the Rice–Ramsperger–Kassel–Marcus (RRKM) theory and transition state theory (TST) continue to be of immense value in terms of their conceptual elegance and ease of application, the deviations from these paradigms due to incomplete IVR can lead to a deeper understanding of reaction dynamics and control (6, 7). Recent studies in both gas (8, 9) and condensed phases (10, 11) indicate that a detailed knowledge of the mechanism of IVR is a prerequisite for formulating dynamically consistent rate theories and, possibly, novel control strategies. Despite the challenges that arise due to the sheer complexity and richness of the IVR process (1), significant advances have been made over the past couple of decades, using a combination of innovative experimental techniques (12, 13) and novel theoretical approaches (14, 15).

The present work focuses on one such novel theoretical approach, based on an analogy between IVR and the phenomenon of Anderson localization, proposed in the seminal work of Logan and Wolynes (16). The so-called state space model describes IVR as a diffusive process in the zeroth-order quantum number space (QNS) (also known as the state space) mediated by the various anharmonic resonances coupling the zeroth-order states. The initial (16) analogy was developed further in a series of important studies (17–19), leading to the local random matrix theory (LRMT) (20) and the equivalent Bose statistics triangle rule (BSTR) (21)—models that have proved to be highly successful in a wide variety of systems ranging from gas phase reaction dynamics (4) to energy flow in proteins (22).

State Space Model of IVR

Consider a molecule with s-vibrational degrees of freedom (df). At sufficiently low energies the Hamiltonian H_0 describes the system as a set of uncoupled oscillators with eigenstates $|\mathbf{v}^{(b)}\rangle \equiv |v_1^{(b)}, v_2^{(b)}, \ldots, v_s^{(b)}\rangle$. The quantity $v_j^{(b)} = 0, 1, 2, \ldots$ is the vibrational quantum number associated with the jth-vibrational mode. Strictly speaking, $|\mathbf{v}^{(b)}\rangle$ are the eigenstates of the best H_0, typically anharmonic and corresponding to nonlinear oscillators. Note that the appropriate H_0 can come from a perturbative analysis of an ab initio surface, taking into account the experimentally observed spectroscopic features, as is the case in the present work (Eq. **5**). Taking the vibrational quantum numbers as the axes, one has the state space (Fig. 1*A*) of the molecule and the dynamics of $|\mathbf{v}^{(b)}\rangle$, a point in the state space, are trivial under H_0—they do not move. However, with increasing energy, the dynamics are dictated by the Hamiltonian $H_0 + V$ with V, consisting of various terms that couple the modes with resonances being key, leading to a nontrivial evolution of $|\mathbf{v}^{(b)}\rangle$ in the state space. This evolution of $|\mathbf{v}^{(b)}\rangle$ mediated by the various anharmonic resonances that manifest locally in the state space is IVR. Depending upon the location of $|\mathbf{v}^{(b)}\rangle$ and the type of resonances that manifest in the QNS, one can have both classical and quantum mechanisms for IVR. The latter mechanism, known as dynamical tunneling (23, 24), has been conjectured (25–27) to be important for polyatomic molecules at low energies with sufficiently high density of states. In the energy regimes and for the class of initial states of interest to

Significance

Facile energy flow among the vibrational modes of a molecule is the primordial step for a reaction. The energy flow pathways are determined by various anharmonic resonances coupling the modes. Assessing the importance of quantum effects like coherence and tunneling to the intramolecular energy flow process requires one to relate the classical pathways mediated by the network of nonlinear resonances, known as the Arnold web, with the quantum pathways. However, very little is known about the ways in which the features of the web can influence the quantum dynamics. In this work we take a significant first step by establishing that a ubiquitous feature of the web, the resonance junction, can slow down the quantum energy flow process.

Author contributions: S.K. designed research; P.M. and S.K. performed research; P.M. and S.K. analyzed data; S.K. wrote the paper; and P.M. contributed to writing *SI Appendix*.

The authors declare no conflict of interest.

*This Direct Submission article had a prearranged editor.

[1]Present address: Center for Information and Communication Technology, Indian Institute of Technology, Jodhpur 342011, India.

[2]To whom correspondence should be addressed. Email: srihari@iitk.ac.in.

This article contains supporting information online at www.pnas.org/lookup/suppl/doi:10.1073/pnas.1406630111/-/DCSupplemental.

Downloaded by guest on January 19, 2022

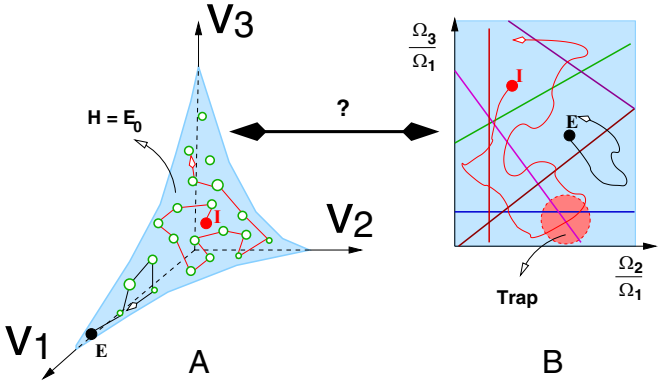

Fig. 1. (*A*) Schematic of the state space (ν_1, ν_2, ν_3) for a 3-df system. Two different initial states *I* and *E* evolve in the state space due to anharmonic resonant couplings. (*B*) Frequency ratio space, a representation of the Arnold web or the network of classical nonlinear resonances (lines), corresponding to *A*. The Ω_j are the nonlinear frequencies. Points in *B* labeled *I* and *E* correspond to those in *A* and evolve on the Arnold web. This work seeks to understand the correspondence between *A* and *B* and the influence of resonance junctions (shaded region in *B*) on the energy flow dynamics.

the current work, however, we do not expect dynamical tunneling to be dominant (*SI Appendix*, Figs. S1 and S4).

A striking prediction (17–19) of the state space model is that at intermediate timescales the survival probability $P_b(t)$ associated with $|\mathbf{v}^{(b)}\rangle$ exhibits power law scaling

$$P_b(t) \equiv \left| \left\langle \mathbf{v}^{(b)} \middle| \mathbf{v}^{(b)}(t) \right\rangle \right|^2 \sim \sigma_b + (1-\sigma_b)\left[1+\frac{2t}{\tau D_b}\right]^{-D_b/2}. \qquad [1]$$

In the above, D_b is the effective dimension of the QNS explored by $|\mathbf{v}^{(b)}\rangle$; σ_b, the dilution factor, is the long time limit of $P_b(t)$; and τ is a timescale associated with an exponential fall-off of $P_b(t)$. Note that σ_b^{-1} yields the total number of zeroth-order states that participate in the IVR dynamics of $|\mathbf{v}^{(b)}\rangle$. In the limit of $D_b = s$, and for large s, the scaling in Eq. **1** is essentially exponential, in accordance with the RRKM expectation. However, and surprisingly, the finding (28, 29) that D_b is significantly smaller than the full dimensionality of the QNS even for fairly large molecules and at significant levels of excitation suggests that correlated intermediate time dynamics might be a generic feature of IVR. Consequently, D_b is a more appropriate descriptor of the IVR dynamics than a simple IVR rate extracted from an exponential fit. This observation, apart from being important for coherent control strategies, raises issues related to the mechanistic origins of D_b being much less than s and to a priori predict D_b for specific initial states. A smoothed version of Eq. **1**, extensively used in this work, is the temporal autocorrelation function (30)

$$C_b(T) = \frac{1}{T}\int_0^T P_b(t)dt, \qquad [2]$$

studied earlier in various contexts. It can be shown that, given Eq. **1**, to leading order $C_b(T) \sim T^{-\delta_b/2}$ with $\delta_b = D_b$ for $0 < D_b < 2$ (*SI Appendix*).

Wong and Gruebele provided a perturbative estimate (31)

$$D_b \approx \frac{\Delta \ln \sum_i L_{ib}^2}{\Delta \ln Q}, \qquad [3]$$

with the sum restricted to states $|i\rangle$ at a distance Q from $|\mathbf{v}^{(b)}\rangle$; i.e., $|\mathbf{v}^{(i)} - \mathbf{v}^{(b)}| \le Q$. The quantity

$$\sum_i L_{ib}^2 \equiv N_{\mathrm{loc}}(b) = \sum_i \left[1+\left(\frac{E_i^0 - E_b^0}{\langle \mathbf{v}^{(i)}|V|\mathbf{v}^{(b)}\rangle}\right)^2\right]^{-1} \qquad [4]$$

is the number of zeroth-order states locally coupled to $|b\rangle$ and signals the onset of facile IVR for $N_{\mathrm{loc}} \ge 1$. Although Eq. **3** ignores contributions from dynamical tunneling, suitably averaged versions do correlate well with D_b. Generically, Eq. **3** predicts slower IVR for states located at the edge of the QNS (overtone modes) compared with states in the interior (combination modes) of the QNS.

There are two crucial questions that we address in this work. First, can certain initial states exhibit multiple power law behavior, not accounted for by Eq. **3**, over different timescales? That is, can D_b vary during the course of evolution (3)? And second, is the nature of the diffusion in the QNS normal or anomalous? The two questions are related because anisotropic exploration results from different sets of anharmonic resonances being active in different regions of the QNS. Thus, degenerate $|\mathbf{v}^{(b)}\rangle$ located at different regions of the QNS can undergo vastly different IVR dynamics, some of them potentially exhibiting anomalous behavior, resulting in strong mode specificity and a changing D_b. As highlighted in the current work, such mode specificity can occur even above the threshold for facile IVR and severely impacts the observations made above in the context of edge vs. interior state dynamics.

State Space–Phase Space Correspondence

Our approach toward answering the questions above involves a detailed classical-quantum correspondence study to establish strong links (Fig. 1) between IVR seen as diffusion in the QNS and IVR manifesting as transport in the classical phase space (32). Indeed, an attractive feature of the state space model is the close classical–quantum correspondence that it affords, allowing one to assess the importance of quantum effects in the IVR dynamics. Valuable insights into the mechanism of IVR have already come from classical–quantum correspondence studies (14, 33) of systems with 2 df in terms of the role of various phase space structures including the chaotic sea, robust Kolmogorov–Arnold–Moser (KAM) barriers, and partial barriers like cantori. However, obtaining similar detailed insights for systems with $s \ge 3$, even classically, presents technical and conceptual challenges (32, 34) that need to be overcome before addressing the more subtle issue of whether the classical IVR mechanisms survive quantization. For instance, KAM tori are no longer barriers to transport and there are no obvious generalizations of the notion of cantori. Moreover, an understanding of "stickiness," arising from trajectories spending long times near regular regions, leading to significant dynamical correlations, remains in its infancy (35). The present work is a first step toward bringing the valuable insights afforded by the classical–quantum correspondence approach to systems with $s \ge 3$ and a key ingredient of our study is the construction, visualization, and interpretation of the dynamics on the classical resonance network, also known as the Arnold web (36). Starting with the pioneering work of Martens et al. (37), several studies (38–46) have amply demonstrated the power of such an approach.

To set the stage for the rest of this paper, we refer to Fig. 1*B*, highlighting two of the important features that distinguish $s \ge 3$ systems from $s < 3$ systems. First, the resonances are not isolated and their associated chaotic layers form a connected network with the possibility of slow transport along the resonances, a phenomenon known as Arnold diffusion. Second, there exist resonance junctions wherein, owing to the exploration of different resonances, a sudden change in the character of the dynamics can occur. Presently, we do not study Arnold diffusion because, apart from the fact that we are not in the near-integrable limit, the timescale necessary for observing it is exceedingly long

Downloaded by guest on January 19, 2022

compared with the quantum power law timescale. In addition, one expects (26, 47, 48) quantum localization of Arnold diffusion for $s = 3$. However, the focus of the current work is on the influence of the resonance junctions because, in the so-called Nekhoroshev regime, one expects the junctions to slow the dynamics down and hence act as a sort of local trap (49–51). Although the regimes of interest studied here are strictly not in the Nekhoroshev regime, our numerical studies show that some of the intriguing quantum results can be unambiguously linked to the slowing down of the dynamics near the resonance junctions. We emphasize that our focus on the local dynamics near the junction implies that Arnold diffusion, if existent, is not dominant because the maximum extent of Arnold diffusion can be observed only away from the junctions (50, 52).

Results and Discussion

Model System and Hamiltonian. We use an effective Hamiltonian for $SCCl_2$, sufficiently accurate for energies of interest (53), obtained (54) by applying canonical Van Vleck perturbation theory to the ab initio Hamiltonian. The resulting Hamiltonian $H = H_0 + V_{\rm res}$ is expressed as

$$H = \sum_{i=1}^{6} \omega_i \left(v_i + \frac{1}{2}\right) + \sum_{i \le j}^{6} x_{ij} \left(v_i + \frac{1}{2}\right)\left(v_j + \frac{1}{2}\right) + V_{\rm res}, \quad [5]$$

with the zeroth-order anharmonic part H_0 characterized by the normal mode frequencies $\{\omega_i\}$ and anharmonicities $\{x_{ij}\}$. The off-diagonal term $V_{\rm res} = \mathcal{V} + \mathcal{V}^\dagger$ consists of six dominant anharmonic resonances coupling the zeroth-order modes with

$$\begin{aligned}\mathcal{V} = {} & k_{526} a_5 a_2^\dagger a_6^\dagger + k_{156} a_1 a_5^\dagger a_6^\dagger + k_{125} a_1 a_2 a_5^{\dagger 2} + k_{36} a_3^2 a_6^{\dagger 2} \\ & + k_{231} a_2 a_3^2 a_1^\dagger + k_{261} a_2 a_6^2 a_1^\dagger,\end{aligned} \quad [6]$$

where a_i, $a_i^\dagger$, and $v_i = a_i^\dagger a_i$ are the mode annihilation, creation, and occupation operators, respectively. The various parameter values (*SI Appendix*, Tables S1 and S2) are taken from an earlier work (54) and note that the first three resonances are much larger than the last three resonances. Due to the existence (54) of three conserved quantities (polyads)

$$K = v_1 + v_2 + v_5; \quad L = 2v_1 + v_3 + v_5 + v_6; \quad M = v_4, \quad [7]$$

the system has effectively 3 df ($s = 3$). The Hamiltonian in Eq. **5** is diagonalized in the zeroth-order number basis $\{v_i\}$ to obtain the eigenstates and eigenvalues. Hereafter, we refer to a specific resonance by indicating the modes involved in the resonance. For example, 526 stands for the first resonance in Eq. **6** above.

The classical limit Hamiltonian corresponding to Eq. **5** can be obtained using the Heisenberg correspondence

$$a_k \leftrightarrow \sqrt{I_k}\, e^{-i\phi_k}; \quad a_k^\dagger \leftrightarrow \sqrt{I_k}\, e^{i\phi_k}, \quad [8]$$

with $(\mathbf{I}, \phi)$ being the action-angle variables of the zeroth-order Hamiltonian. The resulting Hamiltonian,

$$H(\mathbf{I}, \phi) = \sum_{k=1}^{6} \omega_k I_k + \sum_{k \le l=1}^{6} x_{kl} I_k I_l + V_{\rm res}(\mathbf{I}, \phi), \quad [9]$$

is a nonlinear, nonintegrable Hamiltonian. As in the quantum case, existence of the classical analog of (K, L, M) can be used to transform the $s = 6$ system in Eq. **9** to a reduced $s = 3$ Hamiltonian (*SI Appendix*, *SI Text*). The reduced system helps in interpreting the dynamics which, nevertheless, are determined by numerically solving the Hamiltonian's equation of motion corresponding to the full $H(\mathbf{I}, \phi)$.

Quantum Dynamics: Anisotropic Dynamics in State Space and Multiple Power Law Scaling. We study the IVR dynamics of a set of near-degenerate states (see *SI Appendix*, Table S3 for a summary of the relevant properties), with $(K, L, M) = (7, 14, 0)$, spanning a 15-cm^{-1} (~0.5 THz) range centered around $\overline{E}_0 = 7{,}868$ cm^{-1} (~236 THz). The states have varying degrees of mode occupancies and hence differing edgeness parameters (53) e_b (*SI Appendix*, Table S3), with $e_b = 1$ being a pure edge state and $e_b = 0$ being a pure interior state. Our choice of the energy range is motivated by several previous observations. First, $\overline{E}_0$ is close to the threshold for facile IVR and thus poses a challenge for classical–quantum correspondence studies. Second, an earlier study (54) on the dynamical assignment of the eigenstates indicates extensive mixing around $\overline{E}_0$. Third, as shown in Fig. 2*B* (*Inset*), the states are rather typical and comprise the majority (53) of the feature states in $SCCl_2$.

Fig. 2 summarizes the quantum IVR dynamics for the near-degenerate states. Fig. 2*B* shows that although δ_b increases with $N_{\rm loc}$ on the average, there is considerable variation in the δ_b values. For instance, a state with $N_{\rm loc} \sim 5$ has $\delta_b \sim 0.9$ whereas another state with $N_{\rm loc} \sim 2$ exhibits $\delta_b \sim 1.7$, which implies fairly rich and complex state space dynamics due to the sensitivity to specific resonances (29). Our computations show that during the course of the IVR dynamics typically two power law timescales are evident, with the latter corresponding to a slower timescale, and thus the δ_b in Fig. 2*B* represent only an average fit. Assuming δ_b to be correlated with the number of locally active resonances in the state space, Fig. 2*B* suggests that some of the states with $N_{\rm loc} \gg 1$ are evolving either toward the edge of the QNS or to regions in the QNS having fewer active resonances with the possibility of intermediate regime quantum beats (3), i.e., recurrences in $P_b(t)$. The former case would confirm the anisotropic diffusion scenario (18) whereas the latter case would require one to identify the mechanism for evolution into the low-diffusion regions of the QNS.

We now focus on two of the states $|E\rangle = |1, 6, 2, 0, 0, 10\rangle$ ($E^0 \sim 7{,}865.6$ cm^{-1}, $e_b \sim 0.52$) and $|I\rangle = |4, 1, 1, 0, 2, 3\rangle$ ($E^0 \sim 7{,}865.9$ cm^{-1}, $e_b \sim 0.33$)—representative examples for multiple power law scaling and nontrivial IVR dynamics, nontrivial because despite $N_{\rm loc}(|I\rangle) \sim 2.5 N_{\rm loc}(|E\rangle)$, $|E\rangle$ explores more of the state space than $|I\rangle$, as evident from Fig. 2 *C* and *D*. Thus, in the QNS, $|E\rangle$ and $|I\rangle$ are more appropriately classified as "edge-like" and "interior-like" states, respectively. Note that there do exist other sets of states (*SI Appendix*, *SI Text* and Figs. S5 and S6) exhibiting multiple power law scaling. The details of the classical–quantum correspondence, however, can be different for each case (*SI Appendix*, *SI Text*). Fig. 2*A* shows that both $|E\rangle$ and $|I\rangle$ exhibit power law behavior at intermediate timescales and undergo extensive fragmentation with about 20 states participating in the IVR (*SI Appendix*, Table S3). However, a striking feature in Fig. 2*A* is the slowing down of the IVR from $|I\rangle$ around 0.7 ps, much before the long-time dilution regime related to the Heisenberg timescale $\tau_H \equiv (2\pi c \langle \Delta E \rangle)^{-1} \sim 2$ ps with $\langle \Delta E \rangle$ being the mean level spacing. Note that $|E\rangle$ also exhibits a similar slowing down but the effect is much more clear in the case of $|I\rangle$, as evident from Fig. 2 *C* and *D*. A crucial observation is that the second timescale for $|I\rangle$ nearly disappears upon removing the 125 resonance (see Fig. 4*A*) with the effect being minimal on $|E\rangle$. Although a previous study (29) has shown that in the regime $0.8 < N_{\rm loc} < 8$ one expects the IVR dynamics to be sensitive to specific resonances in the QNS, the restricted nature of IVR from $|I\rangle$ upon increasing the strength of the 125 resonance is a puzzling result.

How does one explain the puzzling result noted above? Is it a purely quantum effect? In the following sections, motivated by the fact that the classical analog of $C_b(T)$ corresponds well with the quantum results (*SI Appendix*, Fig. S1), i.e., slower rate of exploration of the phase space by $|I\rangle$, we answer the

Downloaded by guest on January 19, 2022

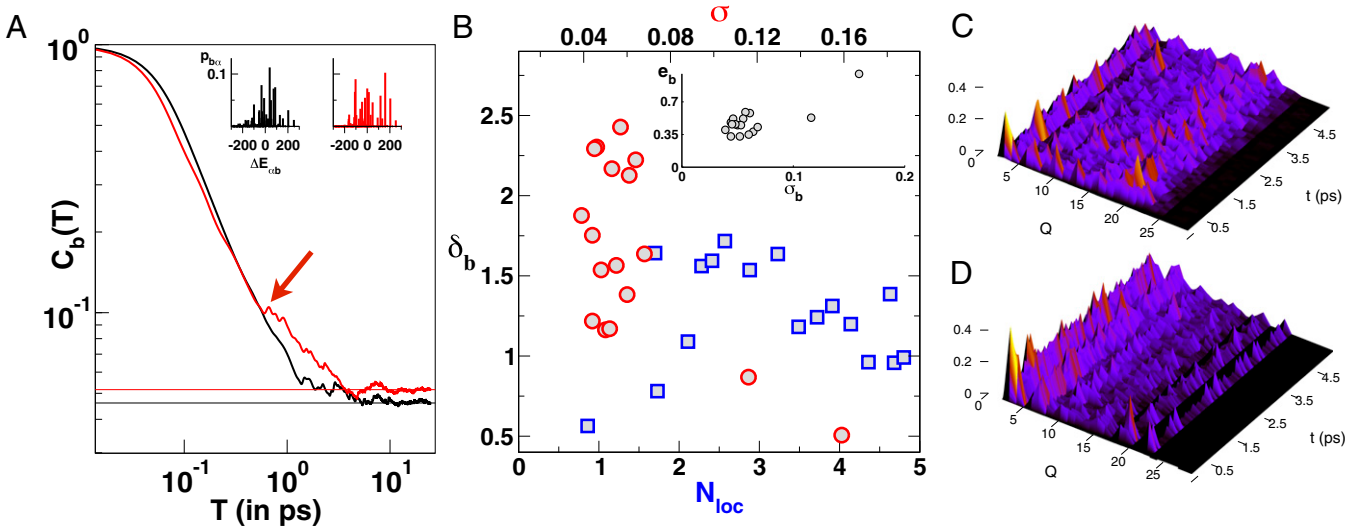

Fig. 2. Summary of the quantum IVR dynamics for $SCCl_2$ with polyads (*K*, *L*, *M*) = (7, 14, 0). (*A*) Time-smoothed survival probabilities for $|E\rangle = |1, 6, 2, 0, 0, 10\rangle$ (black) and $|I\rangle = |4, 1, 1, 0, 2, 3\rangle$ (red) showing substantial slowing down of IVR for $|I\rangle$ starting around $T \sim 0.7$ ps (red arrow). Horizontal lines indicate the long time limit. (*Inset*) Extensive fragmentation of both $|E\rangle$ and $|I\rangle$ due to the various anharmonic resonances. (*B*) Power law exponents δ_b (for Eq. **2**) vs. local number of coupled states N_{loc} (blue squares) and dilution factor σ (red circles) for the near-degenerate states. (*Inset*) Edgeness parameter e_b vs. σ_b for the 17 states of interest with $|E\rangle$ and $|I\rangle$ belonging to the leftmost cluster. (*C* and *D*) Spread of the initial excitation as a function of time and state space distance *Q* for $|E\rangle$ and $|I\rangle$, respectively.

questions by following the IVR dynamics in terms of the nonlinear mode frequencies (37, 43) and reveal significant differences for the two states in terms of the transport behavior on the Arnold web.

Classical Dynamics: Anisotropic IVR on the Resonance Network. The anharmonic mode frequencies of $SCCl_2$, $\Omega^0(\mathbf{I}) \equiv \partial H_0(\mathbf{I})/\partial \mathbf{I}$ in the absence of the resonant couplings, are constant in time. However, in the presence of the resonances $V_{res}(\mathbf{I}, \phi)$ the modes get coupled, actions $\mathbf{I}$ are no longer conserved, and the nonlinear frequencies $\Omega \equiv \Omega^0(\mathbf{I}) + \nabla_{\mathbf{I}} V_{res}(\mathbf{I}, \phi)$ vary with time, exhibiting several mode–mode frequency lockings. Such resonant lockings, key to the observed IVR, are expressed as a condition $\mathbf{r} \cdot \Omega(t) = 0$ with $\mathbf{r} = (r_1, r_2, \ldots, r_6)$ being a resonance vector with mutually prime integer components. In the present case this can be rewritten as

$$\alpha\Omega_{1r}(t) + \beta\Omega_{2r}(t) + \gamma\Omega_{3r}(t) = 0, \qquad [10]$$

in terms of the nonlinear frequencies $\Omega_r(t)$ of the reduced Hamiltonian with (α, β, γ) being integers related to $(r_1, r_2, \ldots, r_6)$. The width of the resonances decreases rapidly with increasing orders, defined by $|\alpha| + |\beta| + |\gamma|$.

A useful way (37, 43) of visualizing the resonance network is to construct the frequency ratio space (FRS) $(f_1, f_2) \equiv (\Omega_{1r}/\Omega_{3r}, \Omega_{2r}/\Omega_{3r})$ in which the resonance lines can be written down as (assuming $\Omega_{3r} \neq 0$)

$$f_2 = -\frac{\alpha}{\beta} f_1 - \frac{\gamma}{\beta}. \qquad [11]$$

Fig. 3*A* shows the resonance network constructed by restricting $(|\alpha| + |\beta| + |\gamma|) \leq 5$ over the dynamical range of (f_1, f_2) at $\overline{E}^0 = 7{,}868\ cm^{-1}$. Such a "static" web highlights the possible resonances and their connectivity that can manifest at the energy of interest. The various near-degenerate states, shown in Fig. 3*B*, are located near $(f_1, f_2) = (0, 0)$, a multiplicity two junction because it is at the confluence of two independent resonances, 156 ($f_1 = 0$) and 526 ($f_2 = 0$). An infinity of resonances emanate from $(f_1, f_2) = (0, 0)$ and, in particular, the 125 resonance corresponds to $f_1 + f_2 = 0$. Several other such junctions, unique to systems with ≥3 df, are clearly seen in Fig. 3*A* and trajectories can diffuse from one junction to another, leading to large-scale transport (55).

Although Fig. 3*A* indicates all possible resonances up to a certain order, it is crucial to know the dynamically relevant regions of the web (39). Such regions can be determined by a joint time-frequency analysis of the classical dynamics. Specifically, the dynamical function $z_k(t) = \sqrt{2I_k(t)}\exp[i\phi_k(t)]$ for a trajectory with initial conditions $(\mathbf{I}_0, \phi_0)$ such that $H(\mathbf{I}_0, \phi_0) = \overline{E}^0$ is subjected to a continuous wavelet transform and the dominant mode frequencies at specific times are obtained (41). Several trajectories are run at the energy of interest and a density plot is generated by recording the number of visits of the trajectories to different regions in the frequency ratio space (see *SI Appendix*, *SI Text* and Figs. S7 and S8 for details on the construction of the density plots).

The computed dynamical FRS at $\overline{E}^0 \approx 7{,}868\ cm^{-1}$ is shown in Fig. 3*B* and the following observations can be made upon comparing to the theoretical web in Fig. 3*A*:

i) The classical IVR dynamics are highly anisotropic with the dominant density being quasi one dimensional along a high-order resonance $f_2 = f_1 - 1/2$ (dashed line in Fig. 3*A*) and parallel to the 261 ($f_2 = f_1$) and the 231 ($f_2 = f_1 - 2$) weak resonances.

ii) The large density near $(f_1, f_2) = (0, 0)$ implies that the dynamics are strongly influenced by the overlap and interplay of the primary 526, 156, and 125 resonances The importance of this junction, in agreement with an earlier quantum study (56), is elaborated below.

iii) The lack of density near the 231 resonance suggests an approximate dynamical decoupling of the a_1-symmetry Cl–C–Cl bend (ν_3). Interestingly, the quantum expectation value $\langle \nu_3(t) \rangle$ for both the states corroborates the classical observation.

iv) The enhanced density near $(f_1, f_2) \sim (-1.9, -2.5)$, far from the primary junction and in a sparse region of the web at this order, implies that higher-order induced resonances are crucial for the long-time IVR dynamics. In particular, the nondiagonal anharmonic terms in Eq. **5** play a significant role.

Downloaded by guest on January 19, 2022

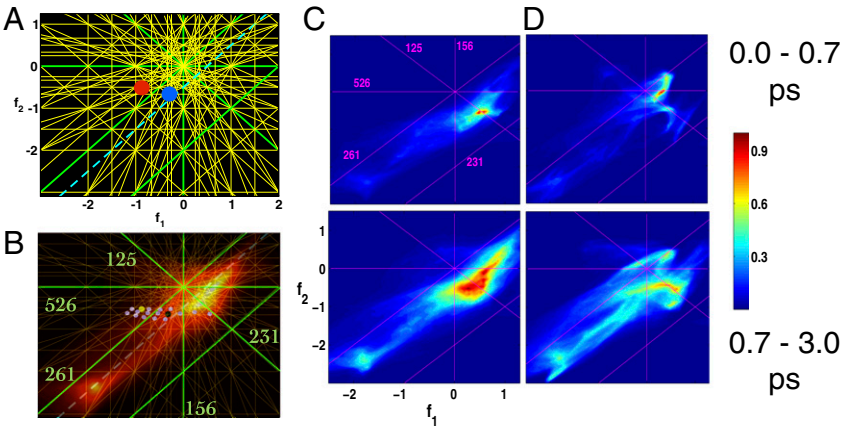

Fig. 3. Summary of the classical IVR dynamics of $SCCl_2$ corresponding to Fig. 2. (*A* and *B*) Classical Arnold web (*A*) and the dynamically dominant part of the web (*B*) at 7,868 cm^{-1} with $(f_1, f_2) \equiv (\Omega_{1r}/\Omega_{3r}, \Omega_{2r}/\Omega_{3r})$. *A* and *B* have identical axes range. The nonlinear resonances (green, labeled in *B*) corresponding to Eq. **6** and other resonances up to a total order of five (yellow lines) are shown. In *A* and *B* the locations of $|E\rangle$ (red), $|I\rangle$ (blue), and the rest of the near-degenerate states are shown, respectively. *C* and *D* show the dynamical evolution of the web for $|E\rangle$ and $|I\rangle$, respectively, over the two timescales of interest as indicated. The dynamics were performed with a total of 10^4 trajectories propagated to 25 ps. All of the plots in *C* and *D* have identical axes range.

Classical–Quantum Correspondence: Anomalous Diffusion and Origin of Multiple Power Law Scaling. According to the LRMT model (17, 18), the microcanonically averaged survival probability at intermediate times is expected to scale as

$$\langle P(t)\rangle \sim \begin{cases} t^{-1} & \text{threshold IVR} \\ t^{-d_f/\alpha} & \text{facile IVR,} \end{cases} \quad [12]$$

with d_f being an effective dimensionality and α characterizing the nature of the diffusion in the state space. Averaging over the 17 near-degenerate states in our case yields $\langle P(t)\rangle \sim t^{-1.4}$ and hence the system is in the facile IVR regime. Assuming normal diffusion ($\alpha = 2$) yields $d_f \sim 2.8$, consistent with an earlier work (56) and close to the full dimensionality $s = 3$ of the QNS. Note that the exponent, extracted over the initial 0.5 ps of the dynamics, is an upper limit because $\langle P(t)\rangle$ exhibits a complicated behavior with beats for $0.5 < t < 2$ ps.

The assumption of normal diffusion, however, requires closer scrutiny because the observed decoupling of the ν_3 bend mode suggests a value of $d_f < 3$. To this end we performed classical and quantum computations (*SI Appendix*, Fig. S2) of the mean squared displacements $\langle (\nu_k(t) - \nu_k(0))^2 \rangle$ for both the states. The results clearly show anomalous behavior in both classical and quantum dynamics with early time ballistic and hyperdiffusive behavior followed by subdiffusive behavior for most of the modes. Consequently, assuming $\max(d_f) \sim 2$ due to the decoupling of the bend mode, we deduce $\alpha \sim 1.4$ and hence an overall anomalous (subdiffusive) state space dynamics at $\overline{E}^0 \approx 7{,}868$ cm^{-1}. An earlier work (44) has implicated sparse regions of the Arnold web with subdiffusive behavior and a recent study shows that tight-binding lattices can exhibit transient quantum hyperdiffusion (57). Hence, the enhanced density around (−1.9, −2.5) in Fig. 3*B*, where the Arnold web is sparse compared with that near (0, 0), combined with the mean squared displacement results clearly establish the subdiffusive nature of the IVR dynamics.

Fig. 3*B* represents the dynamics at $\overline{E}^0 = 7{,}868$ cm^{-1}. However, to compare the dynamics of $|E\rangle$ and $|I\rangle$, we construct their respective FRS by constraining the zeroth-order actions appropriately. In Fig. 3 *C* and *D* the dynamical FRSs of $|E\rangle$ and $|I\rangle$ for the two timescales of interest, motivated by Fig. 2*A*, are shown (see *SI Appendix*, Fig. S3 for the unnormalized data). Remarkably, Fig. 3*D* exhibits a clear change in the nature of the dynamics of $|I\rangle$ in going from the first to the second timescale. The maximum density shifts from the 526 region to the 125 region of the FRS with no such shift for $|E\rangle$. Such a density shift indicates different resonances becoming important at different times during the dynamics, observed for other cases as well (*SI Appendix*, *SI Text* and Fig. S6), and establishes the important role of the classical resonance network in understanding the multiple timescales observed in the quantum dynamics.

The slowing down of IVR from $|I\rangle$ can also be understood from the differences in the structure of the longer-timescale FRS shown in Fig. 3. The $|E\rangle$ density continues to expand across the 526 resonance whereas the $|I\rangle$ density "swirls" around the primary junction. Thus, compared with $|E\rangle$, we suspect that the primary junction is playing a significant role in the IVR dynamics of $|I\rangle$ in terms of trapping the trajectories and leading to slower IVR. To lend further support for the slowing down of the dynamics near the junction, we recall the puzzling observation mentioned earlier regarding the acceleration of IVR for $|I\rangle$ upon removing the 125 resonance. Consequently, we recompute the FRS for $|I\rangle$ with the 125 resonance switched off and the results are shown in Fig. 4*B* at both short and long times. Clearly, the density shift around 0.7 ps is absent and, more interestingly, the long-time FRS shows far less activity around the primary junction. These observations are clearly reflected in the corresponding quantum results shown in Fig. 4*A*, which shows a delayed onset of the second timescale for $|I\rangle$. In addition, as shown in Fig. 4*A*, *Inset*, the removal of the 125 resonance clearly suppresses the recurrences in the survival probability. Thus, we believe that the origin of the slower timescale for $|I\rangle$ in Fig. 2*A* is due to the trapping near

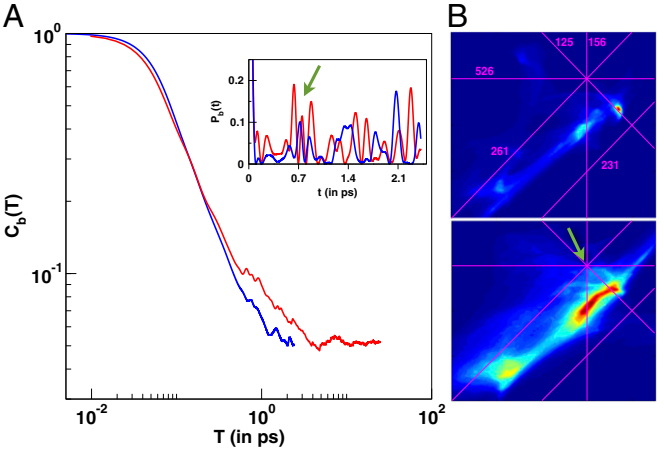

Fig. 4. (*A*) Temporal autocorrelation for $|I\rangle$ in the presence (red) and absence (blue) of the 125 resonance. (*Inset*) Corresponding survival probabilities indicate suppression of the intermediate time recurrences. (*B*) Frequency ratio space in the absence of 125 resonance for $|I\rangle$ at the two timescales as in Fig. 3 (identical axes range). The density shift seen in Fig. 3 disappears and the longer-timescale dynamics exhibit reduced activity near the primary resonance junction.

Downloaded by guest on January 19, 2022

the multiplicity two resonance junction and not due to finite state space effects (*SI Appendix*, Fig. S4).

Conclusions and Future Outlook

In this work we have demonstrated a detailed and remarkable classical–quantum correspondence by showing that a ubiquitous feature of high-dimensional phase spaces, a resonance junction on the Arnold web, is primarily responsible for the slowing down of IVR in the quantum state space. Trapping near resonance junctions is therefore expected (38) to have important ramifications for mode-specific chemistry and control. However, for further progress, several outstanding questions need to be answered and we mention two of them. First, although the influence of higher-order resonances in the Arnold web has been hinted at in this work, the implications of such sparse regions of the web to the quantum ergodicity threshold are largely unexplored and warrant further study in terms of the rate of diffusion near various resonance junctions (52, 58). In this context, apart from more detailed study of the evolution of the Arnold web (59), including the subdominant frequencies in the time-frequency analysis (44) should yield deeper insights. Second, trapping near resonance junctions is one among many possible dynamical barriers that can arise in systems with ≥3 df. Identifying other relevant barriers in the classical phase space and their effect on the quantum IVR dynamics, particularly the potential competition in terms of dynamical tunneling, interference, and localization, is still an open problem.

ACKNOWLEDGMENTS. It is a pleasure to acknowledge Martin Gruebele and David Leitner for insightful comments on this work. P.M. gratefully acknowledges the Indian Institute of Technology, Kanpur, for a graduate fellowship during the time of this research.

1. Nesbitt DJ, Field RW (1996) Vibrational energy flow in highly excited molecules: Role of intramolecular vibrational energy redistribution. *J Phys Chem* 100(31):12735–12756.
2. Keske JC, Pate BH (2000) Decoding the dynamical information embedded in highly mixed quantum states. *Annu Rev Phys Chem* 51:323–353.
3. Gruebele M (2000) Vibrational energy flow: A state space approach. *Adv Chem Phys* 114:193–261.
4. Gruebele M, Wolynes PG (2004) Vibrational energy flow and chemical reactions. *Acc Chem Res* 37(4):261–267.
5. Makarov AA, Malinovsky AL, Ryabov EA (2012) Intramolecular vibrational redistribution: from high-resolution spectra to real-time dynamics. *Physics-Uspekhi* 55(10):977–1007.
6. Lourderaj U, Hase WL (2009) Theoretical and computational studies of non-RRKM unimolecular dynamics. *J Phys Chem A* 113(11):2236–2253.
7. Marcus RA (2013) Theory of mass-independent fractionation of isotopes, phase space accessibility, and a role of isotopic symmetry. *Proc Natl Acad Sci USA* 110(44):17703–17707.
8. Crim FF (2008) Chemical dynamics of vibrationally excited molecules: Controlling reactions in gases and on surfaces. *Proc Natl Acad Sci USA* 105(35):12654–12661.
9. Rehbein J, Carpenter BK (2011) Do we fully understand what controls chemical selectivity? *Phys Chem Chem Phys* 13(47):20906–20922.
10. Glowacki DR, Rose RA, Greaves SJ, Orr-Ewing AJ, Harvey JN (2011) Ultrafast energy flow in the wake of solution-phase bimolecular reactions. *Nat Chem* 3(11):850–855.
11. Assmann J, Kling M, Abel B (2003) Watching photoinduced chemistry and molecular energy flow in solution in real time. *Angew Chem Int Ed Engl* 42(20):2226–2246.
12. Silva M, Jongma R, Field RW, Wodtke AM (2001) The dynamics of "stretched molecules": experimental studies of highly vibrationally excited molecules with stimulated emission pumping. *Annu Rev Phys Chem* 52:811–852.
13. Dian BC, Brown GG, Douglass KO, Pate BH (2008) Measuring picosecond isomerization kinetics via broadband microwave spectroscopy. *Science* 320(5878):924–928.
14. Farantos SC, Schinke R, Guo H, Joyeux M (2009) Energy localization in molecules, bifurcation phenomena, and their spectroscopic signatures: The global view. *Chem Rev* 109(9):4248–4271.
15. Meyer H-D, Gatti F, Worth GA (2009) *Multidimensional Quantum Dynamics: MCTDH Theory and Applications* (Wiley VCH, Weinheim, Germany), 11-30.
16. Logan DE, Wolynes PG (1990) Quantum localization and energy flow in many-dimensional Fermi resonant systems. *J Chem Phys* 93(7):4994–5012.
17. Schofield SA, Wolynes PG (1992) A scaling perspective on quantum energy flow in molecules. *J Chem Phys* 98(2):1123–1131.
18. Schofield SA, Wolynes PG (1995) Rate theory and quantum energy flow in molecules: Modeling the effects of anisotropic diffusion and of dephasing. *J Phys Chem* 99(9):2753–2763.
19. Schofield SA, Wyatt RE, Wolynes PG (1996) Computational study of many-dimensional quantum vibrational energy redistribution. I. Statistics of the survival probability. *J Chem Phys* 105(3):940–952.
20. Leitner DM, Wolynes PG (1997) Vibrational mixing and energy flow in polyatomics: Quantitative prediction using local random matrix theory. *J Phys Chem A* 101(4):541–548.
21. Gruebele M (1996) A Bose-statistics triangle rule model for intramolecular vibrational energy redistribution. *J Phys Chem* 100(30):12183–12192.
22. Leitner DM (2008) Energy flow in proteins. *Annu Rev Phys Chem* 59:233–259.
23. Davis MJ, Heller EJ (1981) Quantum dynamical tunneling in bound states. *J Chem Phys* 75(1):246–254.
24. Keshavamurthy S (2007) Dynamical tunneling in molecules: Quantum routes to energy flow. *Int Rev Phys Chem* 26(4):521–584.
25. Heller EJ, Davis MJ (1981) Quantum dynamical tunneling in large molecules. A plausible conjecture. *J Phys Chem* 85(4):308–309.
26. Heller EJ (1995) Dynamical tunneling and molecular spectra. *J Phys Chem* 99:2625–2634.
27. Leitner DM, Wolynes PG (1996) Many-dimensional quantum energy flow at low energy. *Phys Rev Lett* 76(2):216–219.
28. Gruebele M (1998) Intramolecular vibrational dephasing obeys a power law at intermediate times. *Proc Natl Acad Sci USA* 95(11):5965–5970.
29. Bigwood R, Gruebele M, Leitner DM, Wolynes PG (1998) The vibrational energy flow transition in organic molecules: Theory meets experiment. *Proc Natl Acad Sci USA* 95(11):5960–5964.
30. Ketzmerick R, Petschel G, Geisel T (1992) Slow decay of temporal correlations in quantum systems with Cantor spectra. *Phys Rev Lett* 69(5):695–698.
31. Wong V, Gruebele M (1999) How does vibrational energy flow fill the molecular state space? *J Phys Chem A* 103(49):10083–10092.
32. Keshavamurthy S (2013) Scaling perspective on intramolecular vibrational energy flow: Analogies, insights, and challenges. *Adv Chem Phys* 153:43–110.
33. Uzer T, Miller WH (1991) Theories of intramolecular vibrational-energy transfer. *Phys Rep* 199(2):73–146.
34. Toda M, Komatsuzaki T, Konishi T, Berry RS, Rice SA (2005) Geometric structures of phase space in multidimensional chaos: Applications to chemical reaction dynamics in complex systems. *Adv Chem Phys* 130:1–542.
35. Bunimovich LA (2008) Relative volume of Kolmogorov-Arnold-Moser tori and uniform distribution, stickiness in Hamiltonian systems. *Nonlinearity* 21(2):T13–T17.
36. Lichtenberg AJ, Lieberman MA (1992) *Regular and Chaotic Dynamics* (Springer, New York), pp 373–456.
37. Martens CC, Davis MJ, Ezra GS (1987) Local frequency analysis of chaotic motion in multidimensional systems: Energy transport and bottlenecks in planar OCS. *Chem Phys Lett* 142(6):519–528.
38. Engel YM, Levine RD (1989) Vibration-vibration resonance conditions in intramolecular classical dynamics of triatomic and larger molecules. *Chem Phys Lett* 164(2):270–278.
39. Laskar J (1993) Frequency analysis for multi-dimensional systems. Global dynamics and diffusion. *Physica D* 67:257–281.
40. von Milczewski J, Diercksen GH, Uzer T (1996) Computation of the Arnol'd web for the hydrogen atom in crossed electric and magnetic fields. *Phys Rev Lett* 76(16):2890–2893.
41. Vela-Arevalo LV, Wiggins S (2001) Time-frequency analysis of classical trajectories of polyatomic molecules. *Int J Bifurcat Chaos* 11(5):1359–1380.
42. Bach A, Hostettler JM, Chen P (2005) Quasiperiodic trajectories in the unimolecular dissociation of ethyl radicals by time-frequency analysis. *J Chem Phys* 123(2):021101.
43. Semparithi A, Keshavamurthy S (2006) Intramolecular vibrational energy redistribution as state space diffusion: Classical-quantum correspondence. *J Chem Phys* 125(14):141101.
44. Shojiguchi A, Li C-B, Komatsuzaki T, Toda M (2007) Fractional behavior in multidimensional Hamiltonian systems describing reactions. *Phys Rev E* 76(5):056205.
45. Losada JC, Benito RM, Borondo F (2008) Frequency map analysis of the 3D vibrational dynamics of the LiCN/LiNC molecular system. *Eur Phys J Spec Top* 165:183–193.
46. Paskauskas R, Chandre C, Uzer T (2009) Bottlenecks to vibrational energy flow in carbonyl sulfide: Structures and mechanisms. *J Chem Phys* 130(16):164105–164111.
47. Leitner DM, Wolynes PG (1997) Quantization of the stochastic pump model of Arnold diffusion. *Phys Rev Lett* 79(1):55–58.
48. Demikhovskii VY, Izrailev FM, Malyshev AI (2002) Manifestation of Arnol'd diffusion in quantum systems. *Phys Rev Lett* 88(15):154101.
49. Chirikov BV (1979) A universal instability of many-dimensional oscillator systems. *Phys Rep* 52(5):263–379.
50. Lochak P (1992) Canonical perturbation theory via simultaneous approximation. *Russian Math Surveys* 47(6):57–133.
51. Benettin G, Galgani L, Giorgilli A (1985) Numerical investigations on a chain of weakly coupled rotators in the light of classical perturbation theory. *Nuovo Cim* 89(2):103–119.
52. Efthymiopoulous C, Harsoula M (2013) The speed of Arnold diffusion. *Physica D* 251(2):19–38.
53. Chowdary PD, Gruebele M (2009) An effective Hamiltonian survey of the anharmonic vibrational state space of $SCCl_2$ up to the dissociation energy. *J Chem Phys* 130(13):134310.
54. Jung C, Taylor HS, Sibert EL, III (2006) Assignment and extraction of dynamics of a small molecule with a complex vibrational spectrum: Thiophosgene. *J Phys Chem A* 110(16):5317–5325.
55. Honjo S, Kaneko K (2005) Structure of resonances and transport in multidimensional Hamiltonian systems. *Adv Chem Phys* 130B:437–463.
56. Sibert EL, III, Gruebele M (2006) Molecular vibrational energy flow and dilution factors in an anharmonic state space. *J Chem Phys* 124(2):024317.
57. Zhang Z, Tong P, Gong J, Li B (2012) Quantum hyperdiffusion in one-dimensional tight-binding lattices. *Phys Rev Lett* 108(7):070603.
58. Haller G (1995) Diffusion at intersecting resonances in Hamiltonian systems. *Phys Lett A* 200(1):34–42.
59. Froeschlé C, Guzzo M, Lega E (2000) Graphical evolution of the arnold web: From order to chaos. *Science* 289(5487):2108–2110.

Downloaded by guest on January 19, 2022